RSC Advances

PAPER

View Article Online
View Journal | View Issue

Cite this: *RSC Adv.*, 2018, **8**, 557

Two new luminescence cadmium coordination polymers constructed by 4,4′-di(4*H*-1,2,4-triazol-4-yl)-1,1′-biphenyl and polycarboxylic acids: syntheses, structures, Fe^{3+} identifying and photo-degradable properties†

Qi Huang,[a] Ji-Han Huang,[a] Lei Gu,[a] Jia-xin Ruan,[a] Ying-Hui Yu *[a] and Jin-Sheng Gao*[ab]

Received 1st October 2017
Accepted 12th December 2017

DOI: 10.1039/c7ra10855a

rsc.li/rsc-advances

Two new Cd centered coordination polymers (CPs), namely, $[Cd_3(L)_{1.5}(1,2,4\text{-btc})(H_2O)_4]\cdot H_2O$ (1) and $[Cd_4(L)_2(1,2,4,5\text{-betc})(H_2O)]\cdot H_2O$ (2) have been synthesized by the reaction of 4,4′-di(4*H*-1,2,4-triazol-4-yl)-1,1′-biphenyl (L), polycarboxylic acids and cadmium nitrate under solvothermal conditions. Their structures were first detected by single crystal X-ray diffraction and further characterized by elemental analysis, IR, TGA and X-ray single crystal/powder diffraction. CP 1 with 1,2,4-H_3btc (1,2,4-benzenetricarboxylic acid) as secondary ligand is a 3D framework with (3,4,5)-connected net topology and the point symbol of $\{4\cdot5^2\cdot6\cdot7\cdot8\}\{4\cdot5^2\cdot6^2\cdot7^3\cdot8^2\}\{5\cdot6\cdot7\}$, while 2 with 1,2,4,5-$H_4$betc (1,2,4,5-benzenetetracarboxylic acid) as secondary ligand displays a (4,6)-connected $\{4^4\cdot6^2\}\{4^8\cdot6^7\}$ topological structure. Both CPs 1 and 2 exhibit luminescence properties and the luminescence could be influenced by certain metal cations. The Fe^{3+} identifying and photo-degradable properties of 1 and 2 were studied.

1 Introduction

As versatile scaffolding materials with ordered structures and modular nature, coordination polymers (CPs) have been extensively studied in recent years. Coordination polymers could be constructed from different building blocks to impart desired functions of magnetism,[1] catalysis,[2] gas absorption,[3,4] luminescence[5] and sensing[6] *etc.* Among these properties, considerable efforts have been focused on CPs-based ions recognition and heterogeneous catalysis due to their great advantages such as their structural and chemical tunability, high sensitivity/efficiency and retrievability.[7] A variety of CPs-based luminescence sensors have been built for detecting organic solvent, aromatic explosives and metal cations.[8] CPs also exhibit promising prospects on catalysis for asymmetric synthesis and photochemical degradation process.

Organic linkers and metal centers are of vital importance in the design and synthesis of metal–organic coordination polymers with the expected structures and properties.[9,10] Considering various organic linkers, triazole and its derivatives emerged as excellent ligands in the construction of novel coordination polymers due to their donor–acceptor polarity and unique coordination geometries for bridging multiple metal sites. On the other hand, aromatic multicarboxylates are also adopted as good building blocks considering their strong coordination ability and rich coordination mode. Herein, we choose a bidentate triazole ligand 4,4′-di(4*H*-1,2,4-triazol-4-yl)-1,1′-biphenyl and two polycarboxylic acids to build CPs.[11–13] As a triazole bridging ligand, 4,4′-di(4*H*-1,2,4-triazol-4-yl)-1,1′-biphenyl (L) is longer than most triazole ligands, which can be applied in the construction of stable frameworks with big cavities.[14] As reported, cadmium centered CPs show excellent luminescence and sensing properties in ion recognition.[15] Taking these into account, we presented here two novel coordination polymers, namely, $[Cd_3(L)_{1.5}(1,2,4\text{-btc})(H_2O)_4]\cdot H_2O$ (1) and $[Cd_4(L)_2(1,2,4,5\text{-betc})(H_2O)]\cdot H_2O$ (2), which were synthesized from L and 1,2,4-H_3btc/1,2,4,5-H_4betc with $Cd(NO_3)_2$ under solvothermal conditions. Their structures were characterized by single-crystal X-ray diffraction analysis, elemental analysis, IR analysis and thermal gravimetric analysis. Their Fe^{3+} identifying and photo-degradable properties were also studied (Scheme 1).

2 Experimental sections

2.1 General methods and materials

All chemicals and reagents were purchased and used as received. The IR spectra were obtained on a Perkin Elmer

[a]*School of Chemistry and Materials Science, Heilongjiang University, Harbin 150080, China. E-mail: yuyinghui@hlju.edu.cn; gaojins@hlju.edu.cn; Fax: +86-431-8519-3421; Tel: +86-431-8516-8481*

[b]*Agricultural College, Heilongjiang University, Harbin 150080, China*

† Electronic supplementary information (ESI) available: Tables S1 and S2 and Fig. S1–S7. CCDC 1577350 and 1577351. For ESI and crystallographic data in CIF or other electronic format see DOI: 10.1039/c7ra10855a

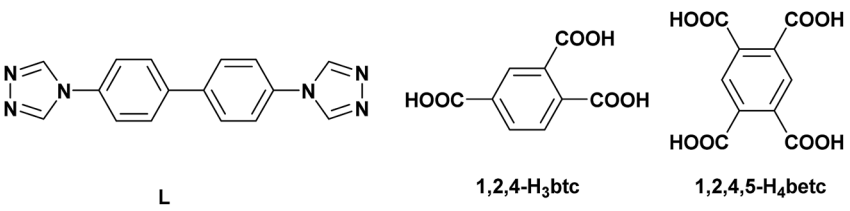

Scheme 1 Structures of L, 1,2,4-H_3btc and 1,2,4,5-H_4betc.

Spectrum 100 FT-IR spectrometer equipped with a DGTS detector (32 scans). The KBr compression method was used with the scanning ranging from 4000 to 500 cm^{-1}. The Perkin-Elmer2400 elemental analyzer was adopted to do the elemental analyses of C, H. Thermogravimetric analyses were carried out with a PerkinElmer STA 6000 with a heating rate of 10 °C min^{-1} under atmosphere from 25 to 800 °C. The PXRD data of the samples were collected on a RigakuD/MAX-3B diffractometer using Cu-Kα radiation ($\lambda = 1.5418$ Å) and 2θ ranging from 5 to 50°. Luminescence spectra were recorded on a Shimadzu RF-5301 spectrophotometer. UV spectra were recorded on a Shimadzu UV-2700 spectrophotometer.

2.2 Synthesis of $[Cd_3(L)_{1.5}(1,2,4\text{-btc})(H_2O)_4]\cdot H_2O$ (1)

The mixture of $Cd(NO_3)_2\cdot 4H_2O$ (31 mg, 0.1 mmol), L (29 mg, 0.1 mmol), 1,2,4-H_3btc (21 mg, 0.1 mmol), imidazole (7 mg, 0.1 mmol, acted as a structure-directing agent (SDA) to obtain bigger size crystals), acetonitrile (2 mL) and H_2O (8 mL) was putted in a 25 mL vial and heated to 140 °C for three days. After cooled to room temperature, the yellow sticky crystals of 1 were separated by filtration. Yield: 55% (based on Cd(II)). Besides, the same kind of single crystals were obtained without adding SDA and the structure was confirmed by PXRD, but the size of these crystals are too small to perform the single crystal diffraction. Elemental analysis (%) calcd for 1 ($C_{42}H_{34}Cd_3N_9O_{17}$): C, 39.59; H, 2.69; N, 9.89; found: C, 38.22; H, 2.59; N, 9.94. IR (solid KBr pellet, cm^{-1}): 3497.1 m,3130.1 w,1545.1 s, 1392.9 s,1096.6 w, 864.1 w,819.8 m,639.4 w,568.8 w, 521.8 w.

2.3 Synthesis of $[Cd_4(L)_2(1,2,4,5\text{-betc})(H_2O)]\cdot H_2O$ (2)

The synthesis method of 2 is similar to that of 1, except that 1,2,4,5-H_4betc was used instead of 1,2,4-H_3btc without imidazole. The colorless rhombus crystals 2 were separated by filtration. Yield: 63% (based on Cd(II)). Elemental analysis (%) calcd for 2 ($C_{52}H_{36}Cd_4N_{12}O_{20}$): C, 39.07; H, 2.27; N, 10.51%; found: C, 38.16; H, 2.13; N, 11.03. IR (solid KBr pellet, cm^{-1}): 3424.8 m, 2087.2 w, 2360.9 w, 1542.1 s, 1380.1 w, 1251.9 w, 1095.6 m, 822.7 w, 766.4 w, 530.5 w.

2.4 X-ray crystallography

Single crystal X-ray diffraction data of CPs 1 and 2 were both collected on a Rigaku R-AXIS RAPID imaging plate diffractometer equipped with graphite-monochromated Mo-Kα (λ = 0.71073 Å), and the test temperature is 291 K. The structures were solved by direct methods and then refined by full-matrix least-squares methods on F^2 using SHELXS-97 crystallographic software package.[16,17] All isolated O atoms have been considered as water atoms. The crystal parameters, refinement results and data collection for 1 and 2 are listed in Table 1.

Table 1 Crystal data and structure refinement for CPs 1 and 2

	1	2
Empirical formula	$C_{42}H_{34}Cd_3N_9O_{17}$	$C_{52}H_{36}Cd_4N_{12}O_{20}$
F_w	1273.98	1598.53
Crystal system	Monoclinic	Monoclinic
Space group	$P2_1/c$	$P2_1/c$
a (Å)	10.188(2)	9.7918(2)
b (Å)	28.963(6)	20.1958(4)
c (Å)	16.627(5)	13.9061(4)
α (deg)	90	90
β (deg)	117.64(2)	112.116(2)
γ (deg)	90	90
V (Å^3)	4346.3(19)	2547.64(10)
Z	4	2
D_{calc} (g cm^{-3})	1.947	2.084
μ (mm^{-1})	1.544	1.745
$F(000)$	2516	1568
Collected/unique	32 304/7632	10 499/4484
R (int)	0.0390	0.0199
GOF on F^2	1.008	1.099
$R_1{}^a$ [$I > 2\sigma(I)$]	0.0278	0.0277
$wR_2{}^b$ [$I > \sigma(I)$]	0.0516	0.0654
$R_1{}^a$ (all)	0.0370	0.0324
$wR_2{}^b$ (all)	0.0530	0.0680

^{a} $R_1 = \sum||F_o| - |F_c||/\sum|F_o|$. ^{b} $wR_2 = \{\sum[w(F_o{}^2 - F_c{}^2)^2/\sum w(F_o{}^2)^2]\}^{1/2}$.

3 Results and discussion

3.1 Structural description

Crystal structure of $[Cd_3(L)_{1.5}(1,2,4\text{-btc})(H_2O)_4]\cdot H_2O$ (1). X-ray analysis reveals that CP 1 crystallizes in the monoclinic system with a $P2_1/c$ space group. The asymmetric unit of CP 1 contains three Cd(II) ions, one and half L molecules, one 1,2,4-H_3btc molecule, four coordinated and one free water molecules. As shown in Fig. 1(a), Cd1, Cd2 and Cd3 atoms all display seven-coordinated geometries. The Cd1 ion is coordinated by one N atom from one L molecule, five O atoms from three $[1,2,4\text{-btc}]^{3-}$ ions and one O atom from one coordinated water molecule. The Cd2 ion is coordinated by two N atoms from two L molecules, four O atoms from two $[1,2,4\text{-btc}]^{3-}$ ions and one O atom from one coordinated water molecule. The Cd3 ion is coordinated by one N atom from one L molecule, four O atoms from three $[1,2,4\text{-btc}]^{3-}$ ions and two O atoms from two coordinated water

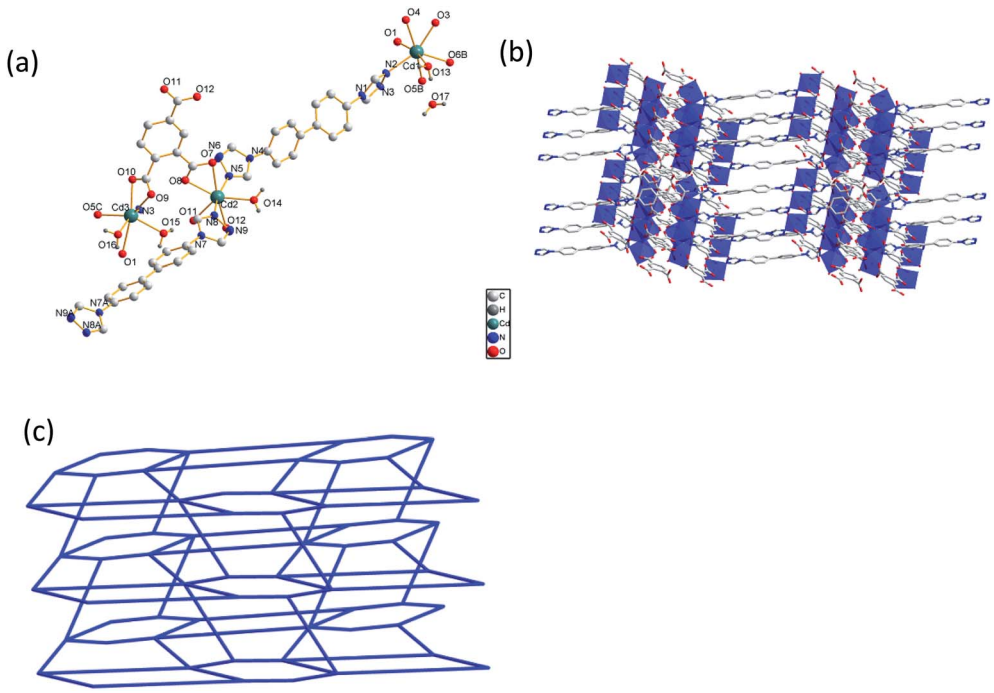

Fig. 1 (a) Stick-ball representation of asymmetric unit of CP 1; (b) 3D framework of CP 1 constructed from 1D chain and 2D network; (c) schematic view of 3D (3,4,5)-connected framework with a point symbol of $\{4\cdot5^2\cdot6\cdot7\cdot8\}\{4\cdot5^2\cdot6^2\cdot7^3\cdot8^2\}\{5\cdot6\cdot7\}$; symmetry code: (A) $1-x, 3-y, 2-z$; (B) $-x, 1-y, 1-z$; (C) $x, 1+y, z$.

molecules. The Cd–N bond lengths range from 2.278(2) to 2.373(2) Å, the Cd–O bond lengths range from 2.2357(19) to 2.595(2) Å, the O–Cd–O bond angles range from 51.89(6) to 171.03(8), the N–Cd–O bond angles are from 74.36(8) to 154.98(8), and the N–Cd–N bond angle is 164.89(9), which are all in the normal ranges.

In CP 1, each L ligand links two Cd(II) ions to form a 1D chain structure, while each $[1,2,4\text{-btc}]^{3-}$ ion links three Cd(II) ions to form a 2D grid-like structure. The chain and grid interweave with each other through sharing the Cd(II) ions to generate a 3D framework (Fig. 1(b)). To better understand the complicated 3D structure of CP 1, topological analysis is carried out.[18] If

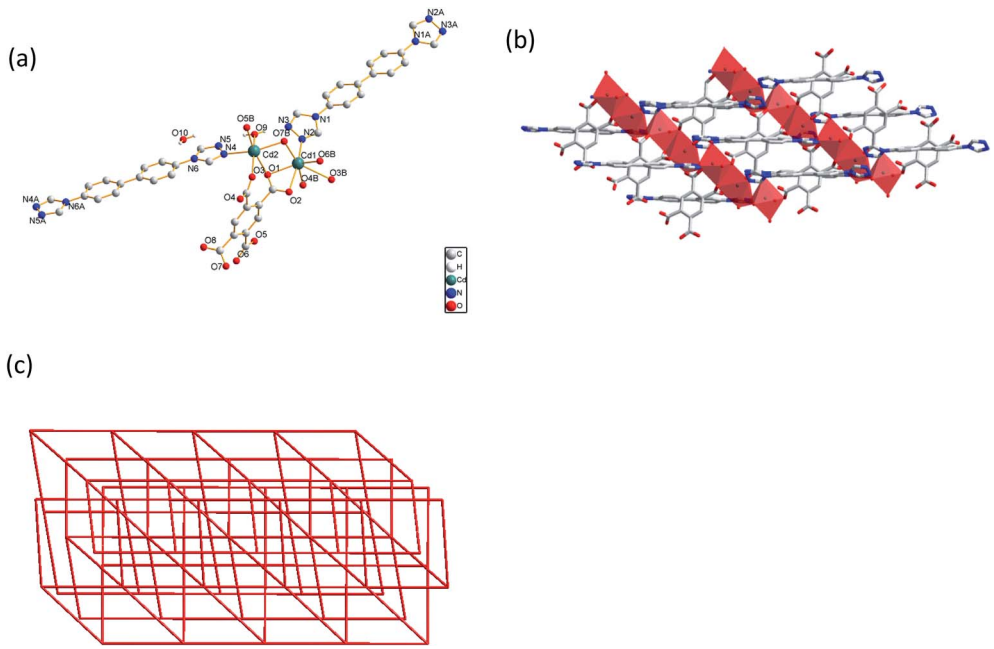

Fig. 2 (a) Stick-ball representation of asymmetric unit of CP 2; (b) 3D framework of CP 2 constructed from 1D chain and 2D twisted network; (c) schematic view of 3D (4,6)-connected framework with a point symbol of $\{4^4\cdot6^2\}\{4^8\cdot6^7\}$; symmetry code: (A) $1-x, -y, -z$; (B) $3-x, -y, 3-z$; (C) $x, 0.5-y, 0.5+z$; (D) $1+x, 0.5-y, 0.5+z$; (E) $1+x, y, z$.

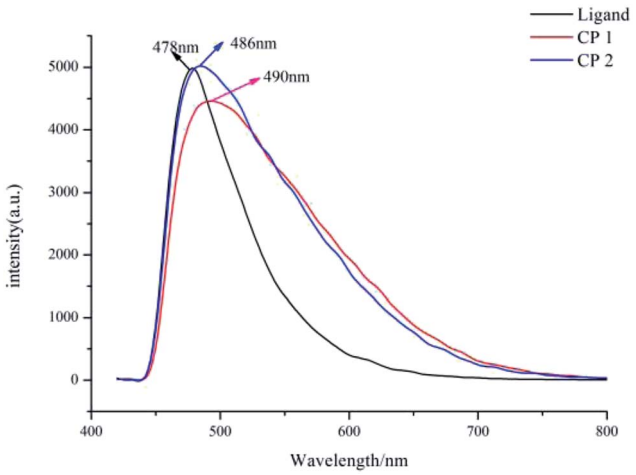

Fig. 3 The solid-state fluorescent emission spectra of free ligand and CPs at room temperature.

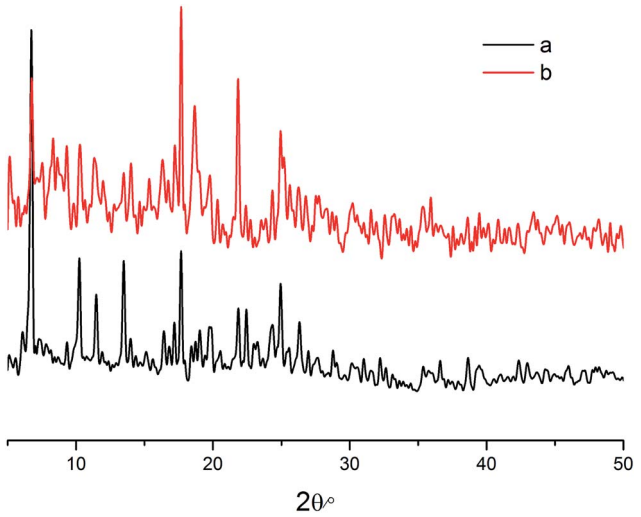

Fig. 5 (a) PXRD pattern of CP 1 before treated with Fe^{3+} ions; (b) PXRD patterns of CP 1 after treated with Fe^{3+} ions.

considering the $[1,2,4\text{-btc}]^{3-}$ ion as a 3-connected node, Cd1 and Cd2 as 5- and 4-connected nodes, respectively, the 3D structure of CP 1 can be seemed as a (3,4,5)-connected net topology with the point symbol of $\{4\cdot5^2\cdot6\cdot7\cdot8\}\{4\cdot5^2\cdot6^2\cdot7^3\cdot8^2\}\{5\cdot6\cdot7\}$ (Fig. 1(c)).

Crystal structure of $[Cd_4(L)_2(1,2,4,5\text{-betc})(H_2O)]\cdot H_2O$ (2). X-ray analysis reveals that CP 2 crystallizes in the same crystal system as CP 1. The asymmetric unit of CP 2 consists of two independent Cd(II) ions, two L ligands, one 1,2,4,5-H_4betc, one coordinated water molecule and one free water molecule. The Cd1 atom also displays seven-coordinating geometry. The Cd1 atom is coordinated by one N atom from one L ligand and six O atoms from three $[1,2,4,5\text{-betc}]^{4-}$ ions. Different from Cd1, the Cd2 atom displays six-coordinating geometry. The Cd2 ion is coordinated by one N from one L ligand, four O atoms from one $[1,2,4,5\text{-betc}]^{4-}$, and one O atom from one coordinated water molecule. The Cd–N bond lengths range from 2.262(3) to

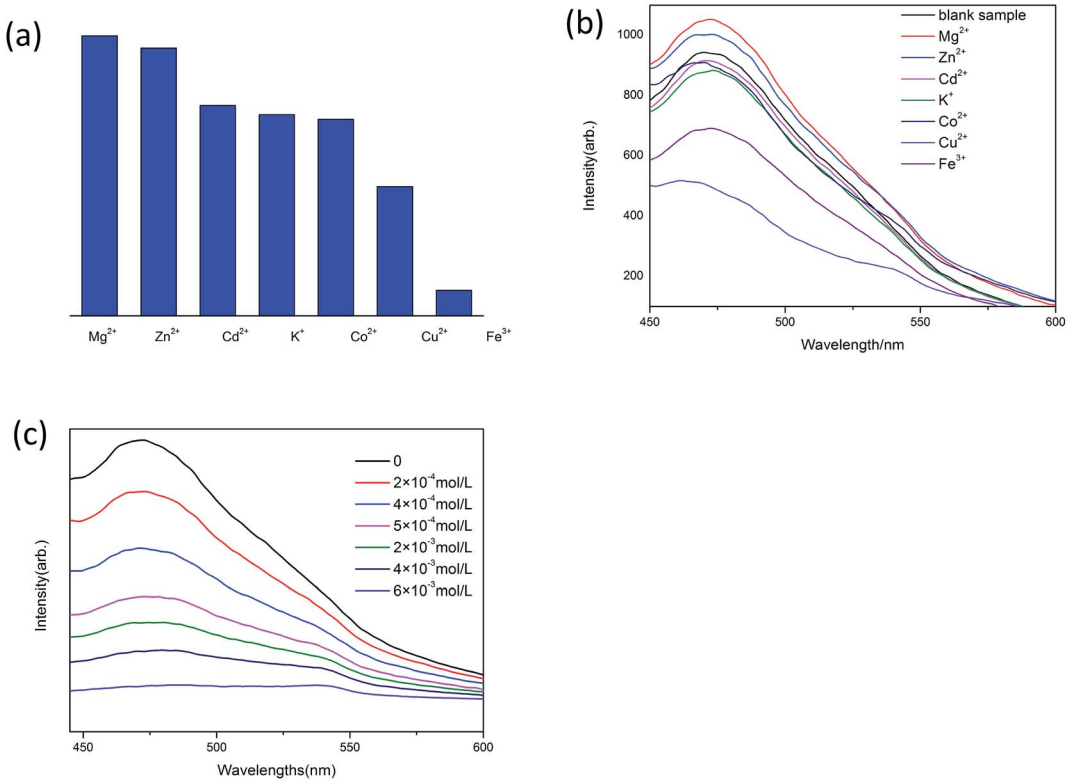

Fig. 4 (a) The relative luminescence intensities of M^{n+}@1 in the mixture of DMF and H_2O; (b) luminescence spectra of 1 with different metal ions; (c) luminescence spectra of Fe^{3+}@1 aqueous suspensions with the concentration of Fe^{3+} in the range 10^{-4}–10^{-3} M.

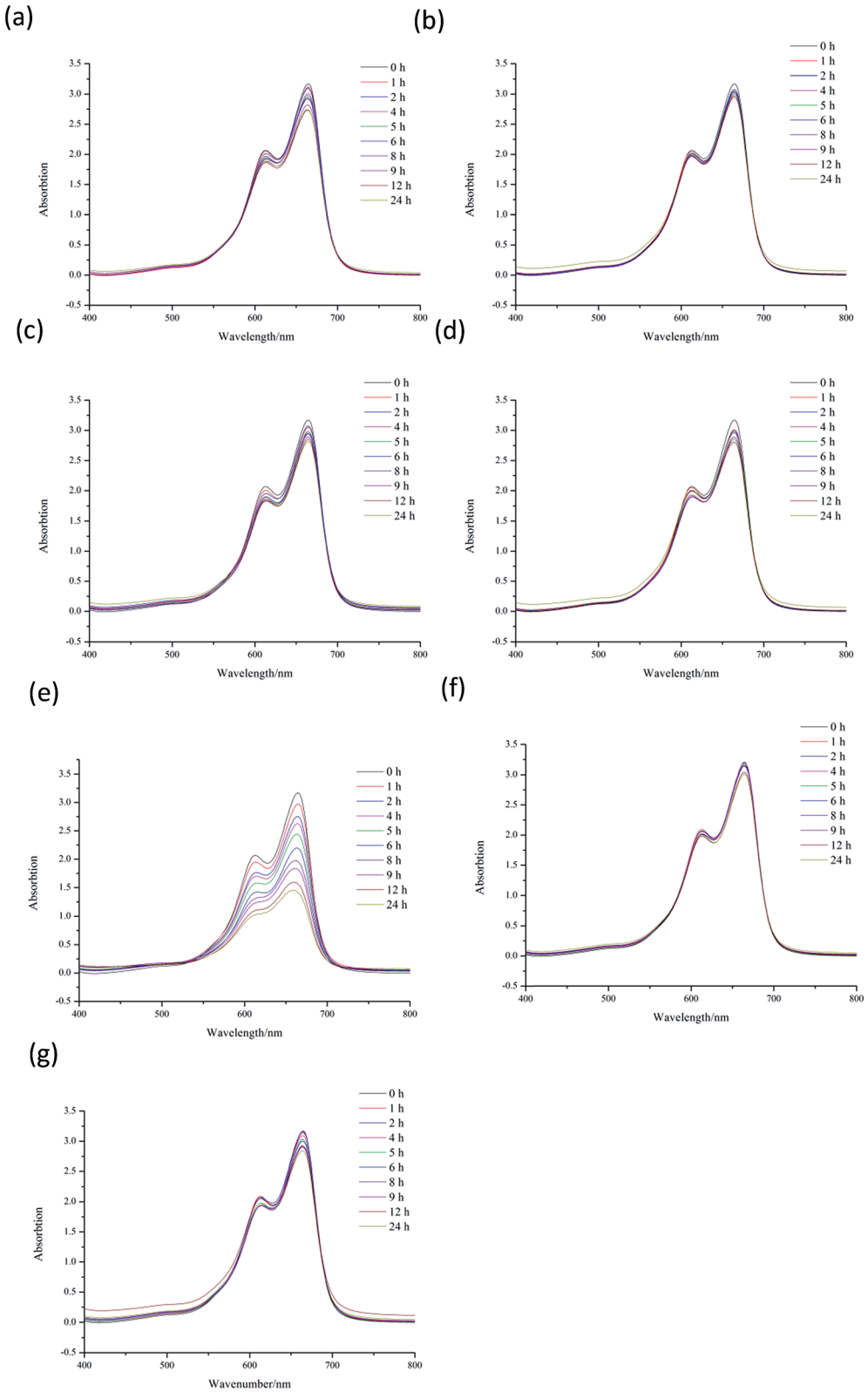

Fig. 6 (a) 2 mL H_2O_2 system under visible light; (b) 5×10^{-4} mol L^{-1} $Cd(NO_3)_2$ system under visible light; (c) 5×10^{-4} mol L^{-1} CP 1 system under visible light; (d) 5×10^{-4} mol L^{-1} $Cd(NO_3)_2$ and 2 mL H_2O_2 system under visible light; (e) 5×10^{-4} mol L^{-1} CP 1 and 2 mL H_2O_2 system under visible light; (f) 5×10^{-4} mol L^{-1} CP 2 system; (g) 5×10^{-4} mol L^{-1} CP 2 and 2 mL H_2O_2 system under visible light.

2.315(3) Å, the Cd–O bond lengths range from 2.233(3) to 2.369(3) Å, the O–Cd–O bond angles range from 54.41(9) to 169.74(10), the N–Cd–O bond angles range from 77.23(11) to 167.82(12), which are all in the normal ranges (Fig. 2(a)).

In CP 2, each ligand links two Cd(II) ions to form a 1D chain structure, while each $[1,2,4\text{-btc}]^{3-}$ ion links four Cd(II) ions to form an infinite extended 2D twisted grid-like structure. The chain and twisted grid interweave with each other through sharing the Cd(II) ions to form a 3D framework (Fig. 2(b)). In order to further analyze and understand the 3D structure of CP 2, topological analysis is carried out. The Cd1 and Cd2 can be considered as 4- and 6-connected nodes. Thus, the network of CP 2 features a (4,6)-connected$\{4^4\cdot6^2\}\{4^8\cdot6^7\}$ topology (Fig. 2(c)).

3.2 PXRD patterns and thermal stability analysis

To investigate the purity of the two CPs, powder X-ray diffraction (Fig. S3 and S4, ESI†) and thermogravimetric analysis (Fig. S5 and S6, ESI†) were carried out. For the two CPs, the peak positions displayed in the experimental patterns are well matched with those in the calculated pattern generated from single crystal diffraction data, indicating that the products are pure CPs. To study the stability of the CPs, thermogravimetric analytical studies were performed. The experiments were conducted on samples of single crystals of 1 and 2 with a heating rate of 10 °C min^{-1}. For CP 1, the whole weight loss of 11.48% between 40 °C and 199 °C is in line with the loss of lattice water molecules (calcd 11.52%). The anhydrous framework begins to disintegrate at 311 °C, the weight loss of 27.19% was observed, owing to the loss of 1,2,4-H_3btc, then the weight loss of 34.13% was observed, owing to the loss of L. The remaining weight of 27.16% corresponds to the formation of CdO. For CP 2, the first weight loss of 3.76% from 40 °C to 212 °C can be ascribed to the loss of two water molecules. On further heating, the framework begins to collapse at 418 °C, which is pretty stable for CPs. The weight loss of 24.36% was observed, owing to the loss of 1,2,4,5-H_4betc, then the weight loss of 37.84% was observed, owing to the loss of L. The remaining weight of 34.04% corresponds to the formation of CdO.

3.3 Photochemical properties

Cadmium CPs attracted a lot of attention for their charming luminescence properties. The luminescence properties of CP 1,

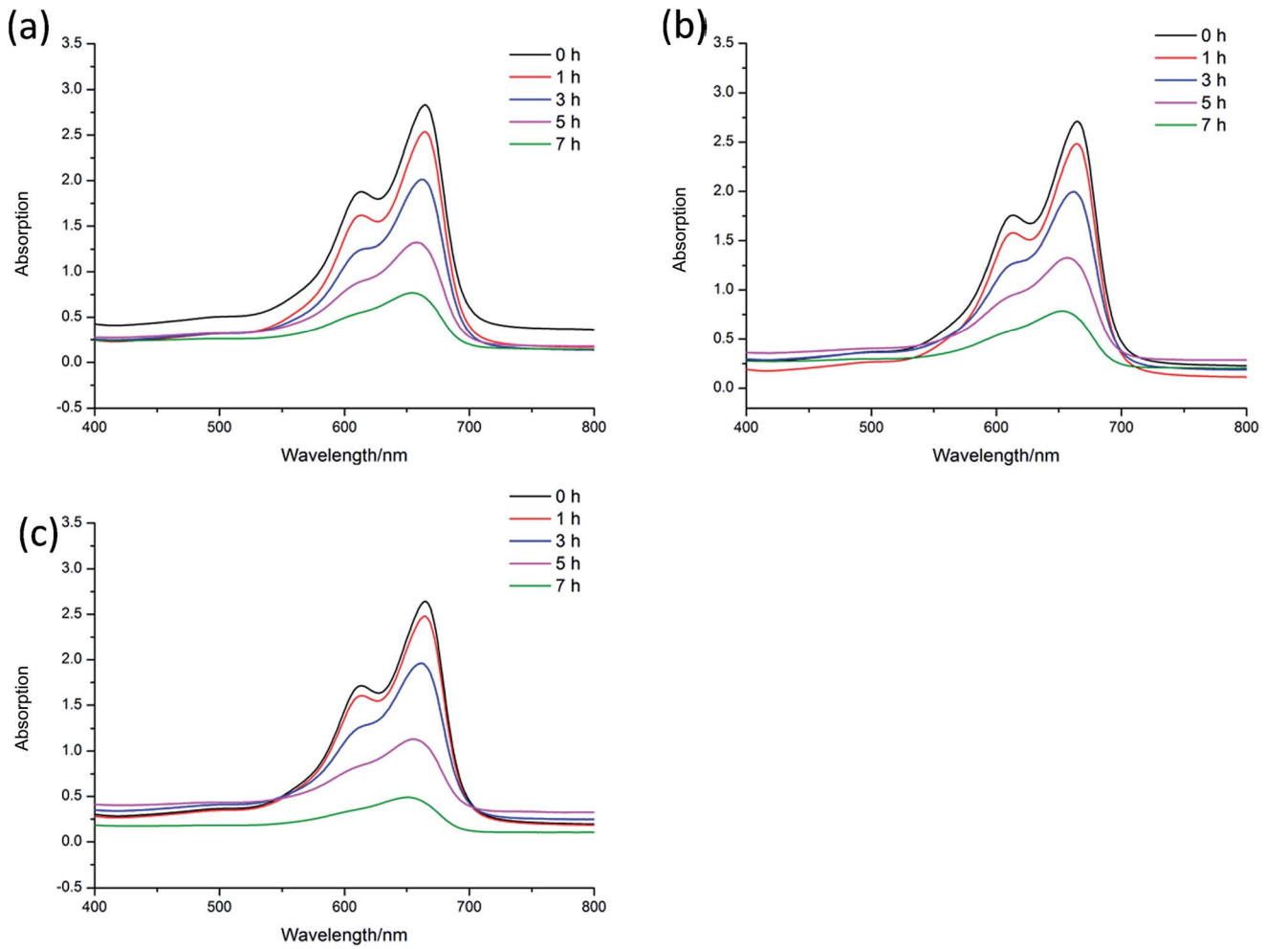

Fig. 7 (a) 5×10^{-4} mol L^{-1} CP 1 and 0.5 mL H_2O_2 system under visible light; (b) 5×10^{-4} mol L^{-1} CP 1 and 1 mL H_2O_2 system under visible light; (c) 5×10^{-4} mol L^{-1} CP 1 and 2 mL H_2O_2 system under visible light.

CP 2 and L in the solid state were measured at room temperature (Fig. 3). In our experiments, the excitation wavelength all fixed to 400 nm. The free ligand has a strong emission at 478 nm, owing to the $\pi \rightarrow \pi^*$ transitions. As we all known, the polycarboxylic acids always assigned to weak $n \rightarrow \pi^*$ transitions, which can be ignored comparing to the $\pi \rightarrow \pi^*$ transitions.[19] So the auxiliary ligand almost has no contribution to the emission of CP 1 and 2. The maximum emission peaks of 1 and 2 are located at 490 nm and 486 nm. The peak shape of CP 1, 2 and the ligand are quite similar, indicating that the luminescence is derived from the ligand.[20] Besides, compared to the free ligand, the weak red-shifts and the obviously widened emission band in 1 and 2 may be attributed to the coordination of ligand to cadmium atoms.

3.4 Fe^{3+} ion identificating properties

The grounded powder samples of CP 1 were immersed in DMF/H_2O solutions with 0.1 mol·L^{-1} $M(NO_3)_n$ (M = Mg^{2+}, Zn^{2+}, Cd^{2+}, K^+, Co^{2+}, Cu^{2+}, Fe^{3+}) and stirred for 12 h to form the M^{n+}@1 for sensing experiments.[21] The luminescence intensities stayed constant on the addition of K^+, Co^{2+} and Cd^{2+} compared to the blank sample, while Mg^{2+}, Zn^{2+}, Cu^{2+} and Fe^{3+} exhibited different quenching effects toward CP 1 depending on the nature of the metal ions (Fig. 4(a) and (b)). Among all the metal ions, CP 1 demonstrates the most significant identifying effect to Fe^{3+} ions. It needs to be emphasized that the luminescence intensities even slightly increased on the addition of Zn^{2+} and Mg^{2+}. On the other hand, same cation recognition effect for CP 2 were also investigated, but the cations' quenching effects toward the luminescence of CP 2 are very poor compared with CP 1. It is might due to the different structures of 1 and 2. CP 2 contains a dual-core closely packed structure, which may have negative effects to the cation recognition.[22–24]

In order to study the relationship between luminescence quenching effect and the concentration of Fe^{3+} ions, we adopted different Fe^{3+} ions concentrations in the range of 10^{-4} to 10^{-3} M (Fig. 4(c)). The experiments show that the luminescence intensities decrease apparently as the concentration of Fe^{3+} ions increases. When the concentration of Fe^{3+} ions reaches 5×10^{-3} M, the luminescence is nearly quenched.

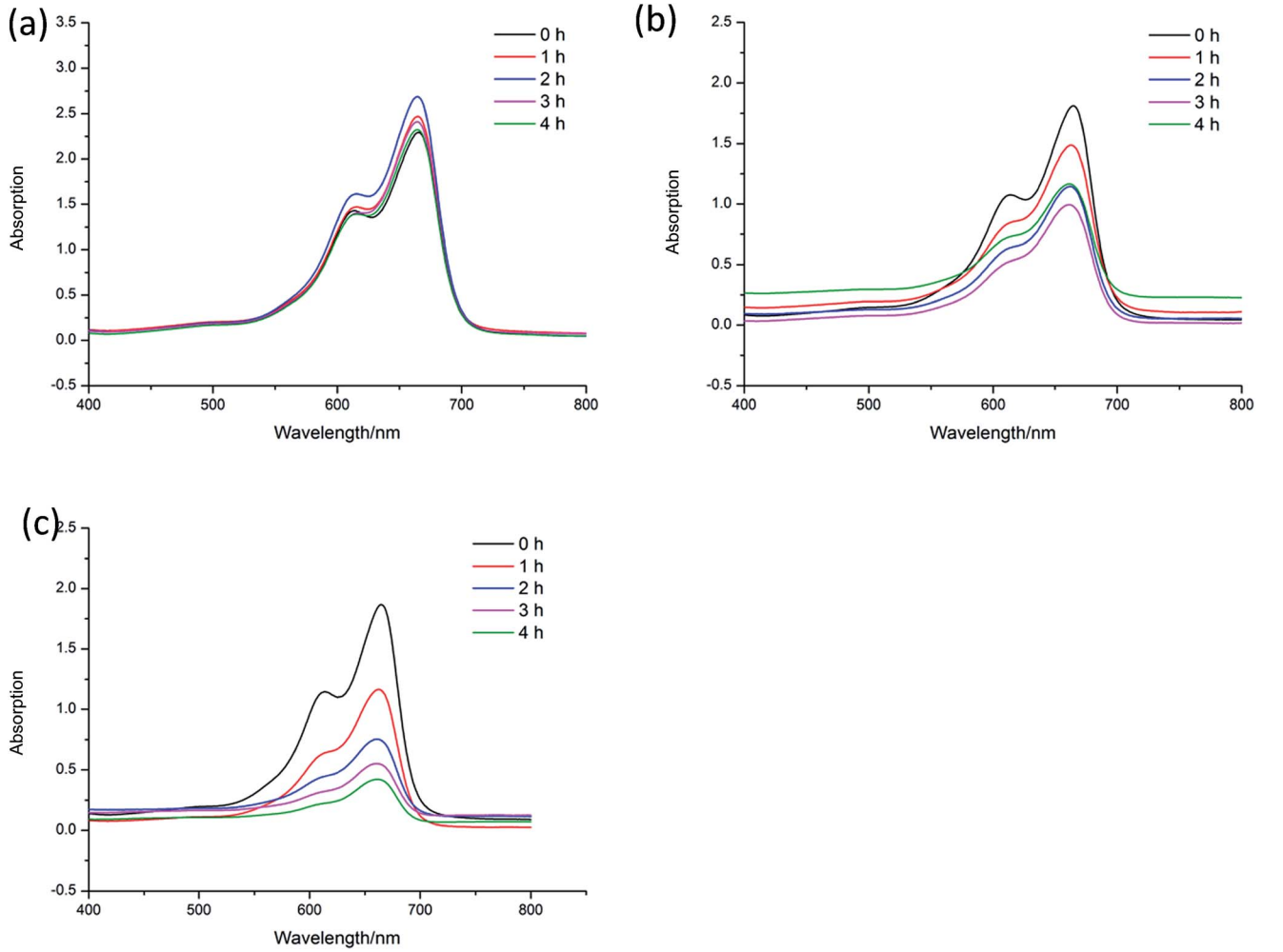

Fig. 8 (a) 5×10^{-4} mol L^{-1} CP 1 and 2 mL H_2O_2 system with the pH value 3 under visible light; (b) 5×10^{-4} mol L^{-1} CP 1 and 2 mL H_2O_2 system with the pH value 8 under visible light; (c) 5×10^{-4} mol L^{-1} CP 1 and 2 mL H_2O_2 system with the pH value 12 under visible light.

At present, the metal ions sensing properties exhibited by the coordination polymers attracted tremendous attention due to their potential application as sensing materials. However, the mechanism of such quenching effect is not very clear to date. Several mechanisms are proposed and presented: (1) the collapse of the framework,[25,26] (2) the ions exchange between the

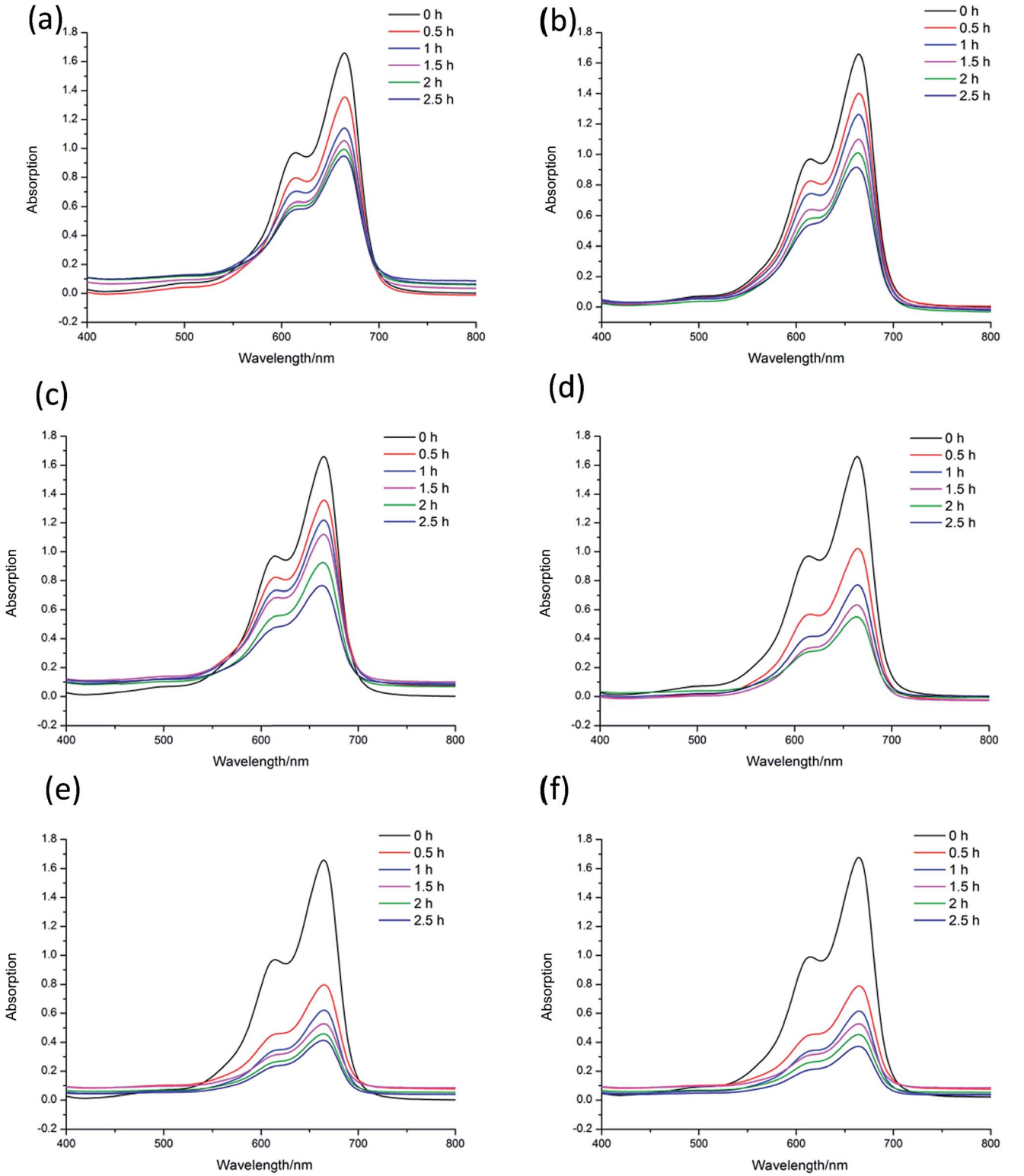

Fig. 9 (a) pH = 12, 2 mL H_2O_2 system under visible light; (b) pH = 12, 2×10^{-5} mol L^{-1} CP 1 and 2 mL H_2O_2 system under visible light; (c) pH = 12, 1×10^{-4} mol L^{-1} CP 1 and 2 mL H_2O_2 system under visible light; (d) pH = 12, 4×10^{-4} mol L^{-1} CP 1 and 2 mL H_2O_2 system under visible light; (e) pH = 12, 8×10^{-4} mol L^{-1} CP 1 and 2 mL H_2O_2 system under visible light; (f) pH = 12, 1×10^{-3} mol L^{-1} CP 1 and 2 mL H_2O_2 system under visible light.

targeted ions and central metal ions of coordination polymers,[27,28] (3) the resonance energy transfer,[29,30] (4) the weak interaction between metal ions and heteroatom within the organic ligands.[31]

In the luminescence quenching process, we found that the metal ions might be included in CP 1 in certain form, which could be confirmed by the color changing of CP 1. CP 1 was originally yellow, however, it changed to brown color after treated with $Fe(NO_3)_3$ solution. Therefore, we carried out PXRD experiments to explore if the framework of CP1 was changed.

After the luminescence quenching process with Fe^{3+}, the samples were centrifuged at 6000 rpm for 3 min, the supernatant and solids were then separated. And the solids were collected and washed with water completely to remove the adsorbed metal ions, then dried for PXRD analysis. The PXRD result was compared with that of the original CP 1. The result showed that the structure of CP 1 changed after the luminescence quenching (Fig. 5).

The different identifying effects toward Fe^{3+} of CP 1 and 2 might be explained by comparing the crystal structures of 1 and 2. As mentioned above, Fe^{3+} quenches the luminescence of CP 1 quite well, while it has no quenching effects to CP 2.[32] Compared with the binuclear CP 2, the trinuclear CP 1 have more uncoordinated oxygen atoms from the polycarboxylic acid and nitrogen atoms from the L which could serve as electron donors. When Fe^{3+} reacts with 1, the lone pair electrons transfer from the oxygen and nitrogen atoms to Fe^{3+} ions to form non-stoichiometric defects. The electrons transferring from the donor to the acceptor results in the luminescence quenching.

3.5 Photo-degradation of MB

Methylene blue (MB) is a kind of dye, which is widely used to make ink, bacterial tissue dyeing and disinfection. However, MB is quite harmful to the ecological environment, especially for the aquatic, such as fish and water plants. Nowadays, the degradation of MB have already attracted the attention of researchers. To investigate the catalytic capacity of CP 1 and 2, a series of experiments of the degradation of MB were carried out. In the following experiments, 15 mg L^{-1} MB aqueous solution were used as samples (50 mL for each sample), and these tests were conducted without any stirring[33] (Fig. 6–10).

The experimental results indicate the systems of H_2O_2, $Cd(NO_3)_2$, CP 1, $Cd(NO_3)_2$–H_2O_2, CP 2 and CP 2–H_2O_2 show no catalytic effects to the degradation of MB. CP 1–H_2O_2 system has obvious catalytic activities to the photo degradation of MB. The CP 2 has pretty poor performance in the MB degradation. CP 1 and 2 are constructed from the reaction of same central metal and ligand with different secondary ligand. The different performance of the two CPs indicated that their diverse 3D structures might have great influence on the catalytic process.[34]

In order to further explore the effects of reaction conditions to the MB degradation, three groups of experiments with different dosage of H_2O_2, pH and the amount of CP 1 were carried out. The result shows that the amount of H_2O_2 has little effect on the degradation efficiency, while pH value

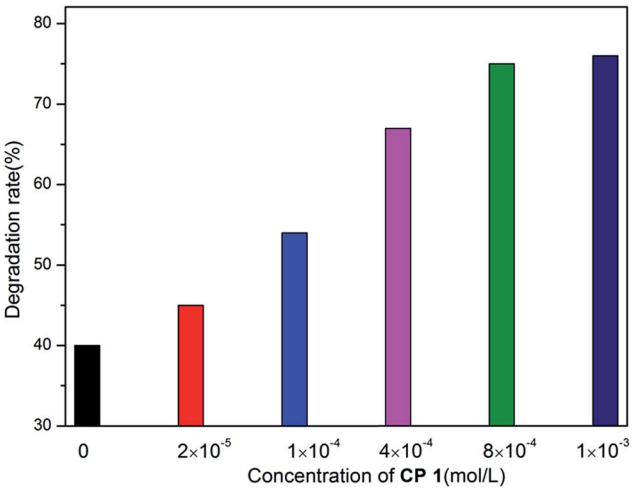

Fig. 10 The degradation rate of MB with the concentration of CP 1 in the range of 0 to 1×10^{-3} mol L^{-1}.

demonstrates great effects in the photo-degradation of MB. When pH value was adjusted to 3, no obvious degradation of MB was observed. When pH value was adjusted to 8, the speed of degradation was moderated. When pH value was increased to 12, nearly 77.3% MB was degraded in 4 h.[35–37] On the basis of the two sets of experiments above, the experiments with different catalyst dosage were also carried out. The catalytic performance of CP 1 increased when the concentration of CP 1 ranged from 0 to 4×10^{-4} mol L^{-1}. However, when the concentration of CP 1 is more than 8×10^{-4} mol L^{-1}, further increasing of the amount of CP 1 have little influence on the reaction. The experimental results indicated that the dosage of CP 1 in certain range could influence the catalytic process, however, when the dosage reached to certain amount (8×10^{-4} mol L^{-1}), such effect became ignorable.

4 Conclusion

In summary, we demonstrated two coordination polymers 1 and 2 from the solvothermal reactions of $Cd(NO_3)_2 \cdot 4H_2O$ and 4,4′-di(4*H*-1,2,4-triazol-4-yl)-1,1′-biphenyl with 1,2,4-H_3btc and 1,2,4,5-H_4betc as the mixed ligand. The presence of different multi-carboxylic acids results in two CPs with diverse topologies, which endows them different performance in Fe^{3+} ion recognition and MB photo-degradation. Compared with the binuclear CP 2, trinuclear CP 1 exhibit better Fe^{3+} ion luminescence sensing effect and photo-degradation catalysis activities toward MB, indicating its potential applications as sensory material for the detection of Fe^{3+} ions and catalyst for photo-degradation process.

Conflicts of interest

There are no conflicts to declare.

Acknowledgements

This work is financially supported by the National Natural Science Foundation of China (Nos. 21371052 & 21501050).

Notes and References

1 M. Kurmoo, *Chem. Soc. Rev.*, 2009, **38**, 1353–1379.
2 A. Dhakshinamoorthy, A. M. Asiri and H. Garcia, *Angew. Chem., Int. Ed.*, 2016, **55**, 5414–5445.
3 M. Eddaoudi, J. Kim, N. Rosi, D. Vodak, J. Wachter, M. O'keeffe and O. M. Yaghi, *Science*, 2002, **295**, 469–472.
4 J. R. Li, R. J. Kuppler and H. C. Zhou, *Chem. Soc. Rev.*, 2009, **38**, 1477–1504.
5 M. D. Allendorf, C. A. Bauer, R. K. Bhakta and R. J. Houk, *Chem. Soc. Rev.*, 2009, **38**, 1330–1352.
6 H. Xu, J. Gao, X. Qian, J. Wang, H. He, Y. Cui, Y. Yang, Z. Wang and G. Qian, *J. Mater. Chem. A*, 2016, **4**, 10900–10905.
7 Y. Q. Huang, H. D. Cheng, H. Y. Chen, Y. Wan, C. L. Liu, Y. Zhao, X. F. Xiao and L. H. Chen, *CrystEngComm*, 2015, **17**, 5690–5701.
8 S. Sanda, S. Parshamoni, S. Biswas and S. Konar, *Chem. Commun.*, 2015, **51**, 6576–6579.
9 O. K. Farha, C. D. Malliakas, M. G. Kanatzidis and J. T. Hupp, *J. Am. Chem. Soc.*, 2009, **132**, 950–952.
10 X. Y. Wan, F. L. Jiang, L. Chen, J. Pan, K. Zhou, K. Z. Su, J. D. Pang, G. X. Lyu and M. C. Hong, *CrystEngComm*, 2015, **17**, 3829–3837.
11 G. A. Senchyk, A. B. Lysenko, E. B. Rusanov, A. N. Chernega, J. Jezierska, K. V. Domasevitch and A. Ozarowski, *Eur. J. Inorg. Chem.*, 2012, **2012**, 5802–5813.
12 G. A. Senchyk, A. B. Lysenko, I. Boldog, E. B. Rusanov, A. N. Chernega, H. Krautscheid and K. V. Domasevitch, *Dalton Trans.*, 2012, **41**, 8675–8689.
13 Y. J. Hu, J. Yang, Y. Y. Liu, S. Song and J. F. Ma, *Cryst. Growth Des.*, 2015, **15**, 3822–3831.
14 Y. Garcia, A. Naik and J. Marchand Brynaert, *Synthesis*, 2008, **2008**, 149–154.
15 Y. J. Yang, M. J. Wang and K. L. Zhang, *J. Mater. Chem. C*, 2016, **4**, 11404–11418.
16 P. Lu, Y. H. Yu, Z. J. Chen, G. F. Hou, Y. M. Chen, D. S. Ma, J. S. Gao and X. F. Gong, *Synth. Met.*, 2015, **203**, 164–173.
17 G. M. Sheldrick, *SHELXS-97, Program for crystal structures solution*, University of Guttingen, Germany, 1997.
18 G. M. Sheldrick, *SHELXL-97, Program for the Refinement of crystal structures*, University of Göttingen, Germany, 1997.
19 W. Chen, J. Y. Wang, C. Chen, Q. Yue, H. M. Yuan, J. S. Chen and S. N. Wang, *Inorg. Chem.*, 2003, **42**, 944–946.
20 S. B. Miao, Z. H. Li, C. Y. Xu and B. M. Ji, *CrystEngComm*, 2016, **18**, 4636–4642.
21 Y. Wu, G. P. Yang, Y. Zhao, W. P. Wu, B. Liu and Y. Y. Wang, *Dalton Trans.*, 2015, **44**, 3271–3277.
22 Y. Wu, G. P. Yang, X. Zhou, J. Li, Y. Ning and Y. Y. Wang, *Dalton Trans.*, 2015, **44**, 10385–10391.
23 R. Kumar, Y. O. Lee, V. Bhalla, M. Kumar and J. S. Kim, *Chem. Soc. Rev.*, 2014, **43**, 4824–4870.
24 J. F. Song, J. J. Luo, Y. Y. Jia, L. D. Xin, Z. Z. Lin and R. S. Zhou, *RSC Adv.*, 2017, **7**, 36575–36584.
25 X. Y. Xu and B. Yan, *ACS Appl. Mater. Interfaces*, 2015, **7**, 721–729.
26 S. Dang, E. Ma, Z.-M. Sun and H. Zhang, *J. Mater. Chem.*, 2012, **22**, 16920.
27 Y. Zhou, H.-H. Chen and B. Yan, *J. Mater. Chem. A*, 2014, **2**, 13691–13697.
28 C. X. Yang, H. B. Ren and X. P. Yan, *Anal. Chem.*, 2013, **85**, 7441–7446.
29 S. Pramanik, C. Zheng, X. Zhang, T. J. Emge and J. Li, *J. Am. Chem. Soc.*, 2011, **133**, 4153–4155.
30 Z. Hu, B. J. Deibert and J. Li, *Chem. Soc. Rev.*, 2014, **43**, 5815–5840.
31 Q. Tang, S. Liu, Y. Liu, J. Miao, S. Li, L. Zhang, Z. Shi and Z. Zheng, *Inorg. Chem.*, 2013, **52**, 2799–2801.
32 G. P. Li, G. Liu, Y. Z. Li, L. Hou, Y. Y. Wang and Z. Zhu, *Inorg. Chem.*, 2016, **55**, 3952–3959.
33 J. Zhang, L. Gong, J. Feng, J. Wu and C. Zhang, *New J. Chem.*, 2017, **41**, 8107–8117.
34 H. R. Yan, J. Wang, Y. H. Yu, G. F. Hou, H. X. Zhang and J. S. Gao, *RSC Adv.*, 2016, **6**, 71206–71213.
35 S. Roy, K. Harms, A. Bauzá, A. Frontera and S. Chattopadhyay, *Polyhedron*, 2017, **121**, 199–205.
36 M. Jahurul Islam, H. K. Kim, D. Amaranatha Reddy, Y. Kim, R. Ma, H. Baek, J. Kim and T. K. Kim, *Dalton Trans.*, 2017, **46**, 6013–6023.
37 C. C. Wang, J. R. Li, X. L. Lv, Y. Q. Zhang and G. Guo, *Energy Environ. Sci.*, 2014, **7**, 2831–2867.